Supplement of Atmos. Chem. Phys., 26, 12671–12687, 2026
https://doi.org/10.5194/acp-26-12671-2026-supplement

Atmospheric Chemistry and Physics
Open Access

Supplement of

Measurement report: Impacts of thermodynamic and dynamic processes on the vertical distribution of carbonaceous aerosols: lessons from in-situ observations at the eastern foothills of Liupan Mountains, Loess Plateau

Shaofeng Qi et al.

Correspondence to: Suping Zhao (zhaosp@lzb.ac.cn)

S1: Analysis methods of WPSCF and WCWT

In the calculation of WPSCF (weighted potential source contribution function) and WCWT (weighted concentration weighted trajectory), we first calculated the air mass trajectories for the preceding 48 hours at heights of 100 m, 500 m, and 1000 m within all observation days (July 15–24, 2023, and July 17–31, 2024). Next, the UVPM mass concentration data were overlaid onto the air mass trajectory data, and the areas traversed by the air mass trajectories were divided into a 0.5°×0.5° grid, in order to determine the potential source regions of UVPM for the observation station. The calculation methods for WPSCF and WCWT are shown in Equations (S1) and (S2) (Wang, 2024):

$$\mathrm{WPSCF}_{ij} = \frac{m_{ij}}{n_{ij}} \times W_{ij} \qquad \text{(S1)},$$

$$C_{ij} = \frac{1}{\sum_{l=1}^{M} \tau_{ijl}} \times \sum_{l=1}^{M} C_l \tau_{ijl} \qquad \text{(S2)}.$$

In Equation (S1), m_{ij} represents the number of polluted trajectory endpoints within the ij-th cell, and n_{ij} represents the total number of trajectory endpoints within the ij-th cell. W_{ij} is the weighting factor. In Equation (S2), C_{ij} is the average weighted concentration in the ij-th cell, l is the index of the trajectory, M is the total number of trajectories, C_l is the concentration observed on arrival of trajectory l, and τ_{ijl} is the time spent in the ij-th cell by trajectory l. A high value for C_{ij} implies that air parcels traveling over the ij-th cell would be, on average, associated with high concentrations at the receptor. The arbitrary weighting function described above was also used in the CWT analyses to reduce the effect of the small values of n_{ij}. (All the above content refers to the official MeteoInfo documentation, which can be found at the following URL: http://www.meteothink.org/docs/trajstat/trajstatrun.html.)

S2: Profile classification method

In classifying the vertical profiles, we performed the cluster analysis based on the gradient variation of eBC (equivalent Black Carbon). The four resulting profile types were defined. Uniformly decreasing (Cluster 1): In the observed samples, the vertical gradient of eBC concentration is less than 0.6 μg m^{-3} km^{-1} and remains nearly constant, exhibiting either a quasi-linear or weakly decreasing trend with height; Non-uniformly decreasing (Cluster 2): In the observed samples, the vertical gradient of eBC concentration exceeds 1.0 μg m^{-3} km^{-1} within the lowest 500 m and persists over a vertical extent of at least 50 m, indicating a more rapid decrease with height; Double-inflection point (Cluster 3): Observation samples where the eBC concentration profile clearly displayed two inflection points, typically characterized by an initial decrease with height, followed by an increase, and then a subsequent decrease; Continuous increasing (Cluster 4): Observation samples where the eBC concentration exhibited a continuous increase with increasing height across the observed column.

S3: Selection guidelines for pollution incidents

1. Diesel vehicle emissions: During the 20:00 observation on July 17, 2024, a diesel harvester was operating approximately 50 m from our observation site and ceased work after about half an hour. Consequently, we define this specific observation as being affected by diesel vehicle emissions. For comparison, we selected the 23:00 observation—which has the shortest temporal difference—as the corresponding non-diesel vehicle emission observation.

2. Dust Pollution: A dust event occurred throughout the entire day of July 21, 2024. We defined the 8:00 observation, when the dust was most severe (PM_{10} concentration in Pingliang urban area was 350 μg m^{-3} at that time), as the dust pollution observation. Since the dust event lasted for a long duration, we chose the observation taken at the same time on the previous day (8:00 on July 20, 2024) for comparison.

S4: Two-component model

Referring to the studies by Chen et al. (2015), we used a two-component model to separate the light absorption coefficients of eBC and UVPM, calculated using the following formulas:

$$b_{Abs,\lambda} = b_{Abs,\lambda,eBC} + b_{Abs,\lambda,UVPM} = A_1 \times \lambda^{-AAE_{eBC}} + A_2 \times \lambda^{-AAE_{UVPM}} \quad \text{(S3)}.$$

Where AAE_{eBC} and AAE_{UVPM} are the Absorption Ångström Exponents (AAE) for eBC and UVPM, respectively. In the calculation process, eBC is typically assumed to be composed of pure carbon, thus AAE_{eBC} is approximated as 1.0 (Chow et al., 2018). The values of A_1, A_2, and AAE_{UVPM} in the equations are then determined through a least-squares fitting method.

Table S1 Methods to calculate the planetary boundary layer height (Holzworth, 1964; Zhang et al., 2020).

Methods	Formulas	Annotation
Air parcel method	$\theta(h_i) = \theta_1$	θ_1 denotes the potential temperature at the lowest model level, corresponding to the surface layer
Potential temperature gradient method	$\frac{d\theta}{dZ}\Big\vert_{Z=h_i} = 0$	

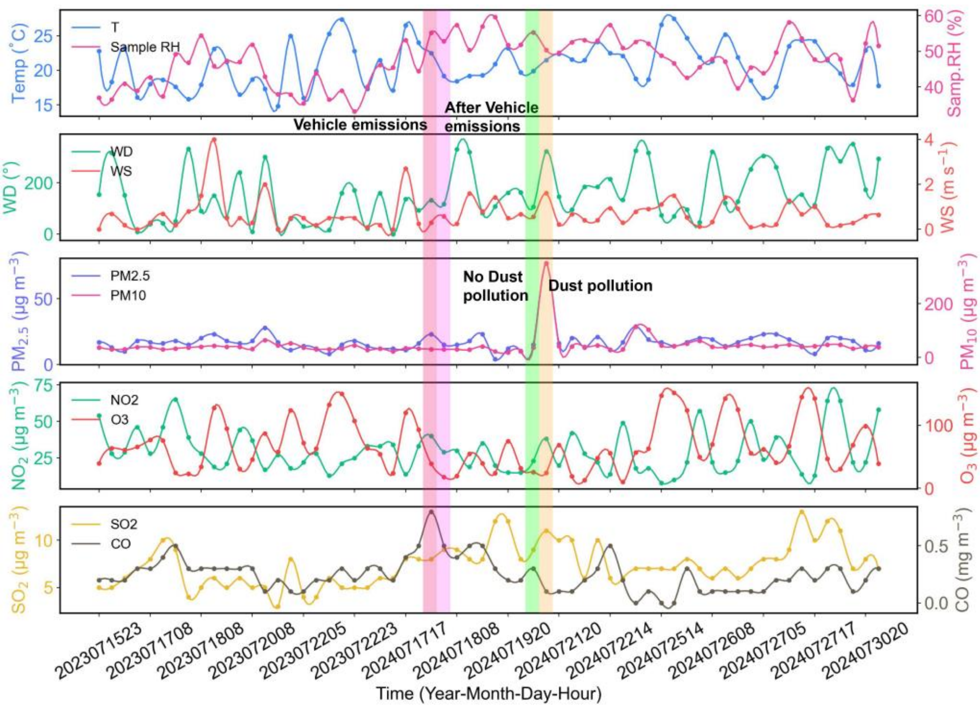

Figure S1. Temporal variations of meteorological parameters, including air temperature (T), relative humidity (RH), wind direction (WD), wind speed (WS), and air pollutants, including particulate matter with aerodynamic diameter smaller than 2.5 μm ($PM_{2.5}$) and than 10 μm (PM_{10}), nitrogen dioxide (NO_2), ozone (O_3), sulfur dioxide (SO_2), and carbon monoxide (CO), were observed during the monitoring period. The shaded areas in the figure represent the during and after vehicle emissions, no dust pollution, and dust pollution at 20:00 on July 17, 23:00 on July 17, 2024, 08:00 on July 20, 2024, 08:00 on July 21, 2024, respectively.

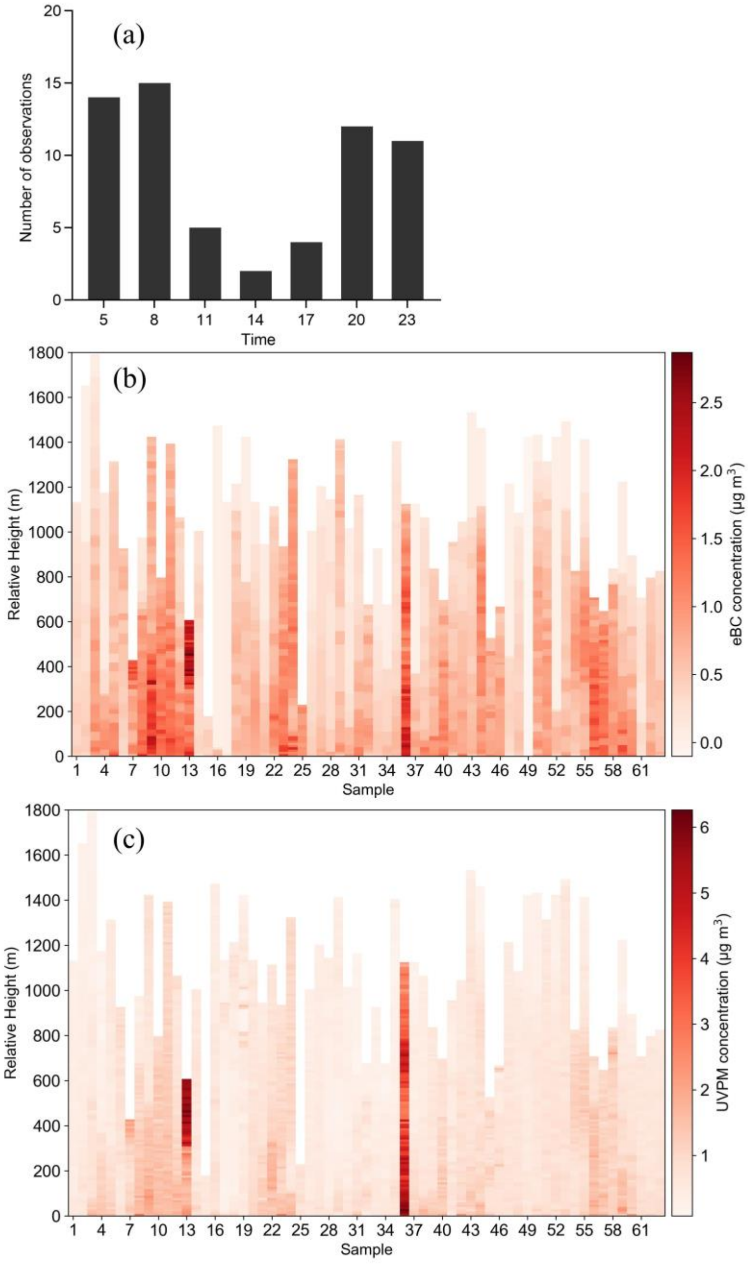

Figure S2. a) Statistics of the number of observations for different hours of day, while b) and c) the observation heights for each measurement and the eBC and UVPM concentrations at different heights, respectively.

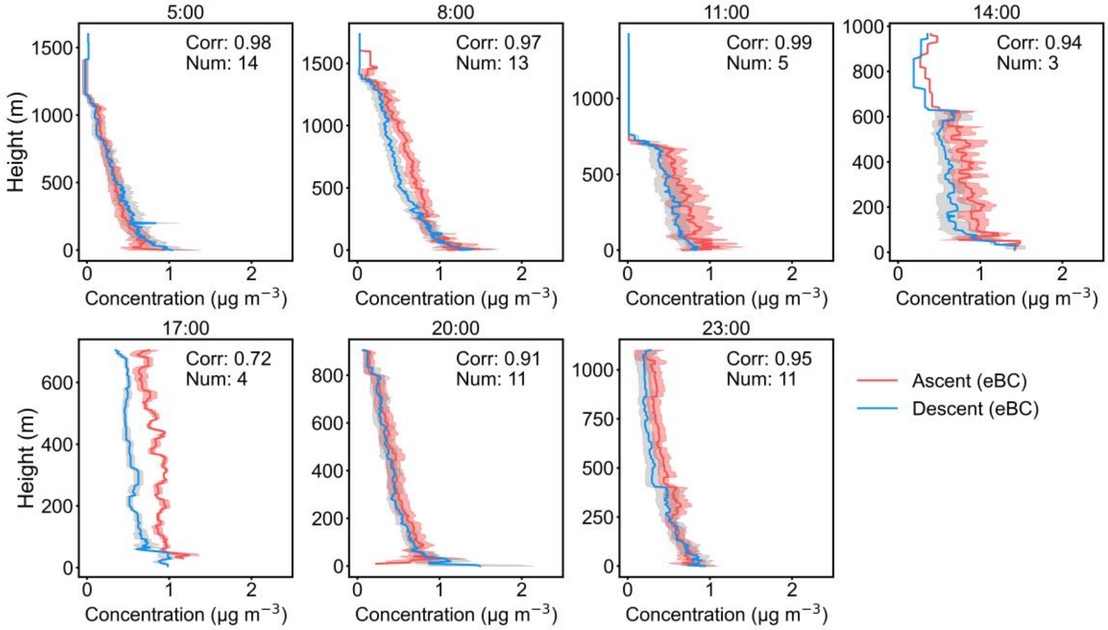

Figure S3. Comparison of equivalent black carbon (eBC) vertical profiles during ascent with those during descent of the tethered balloon.

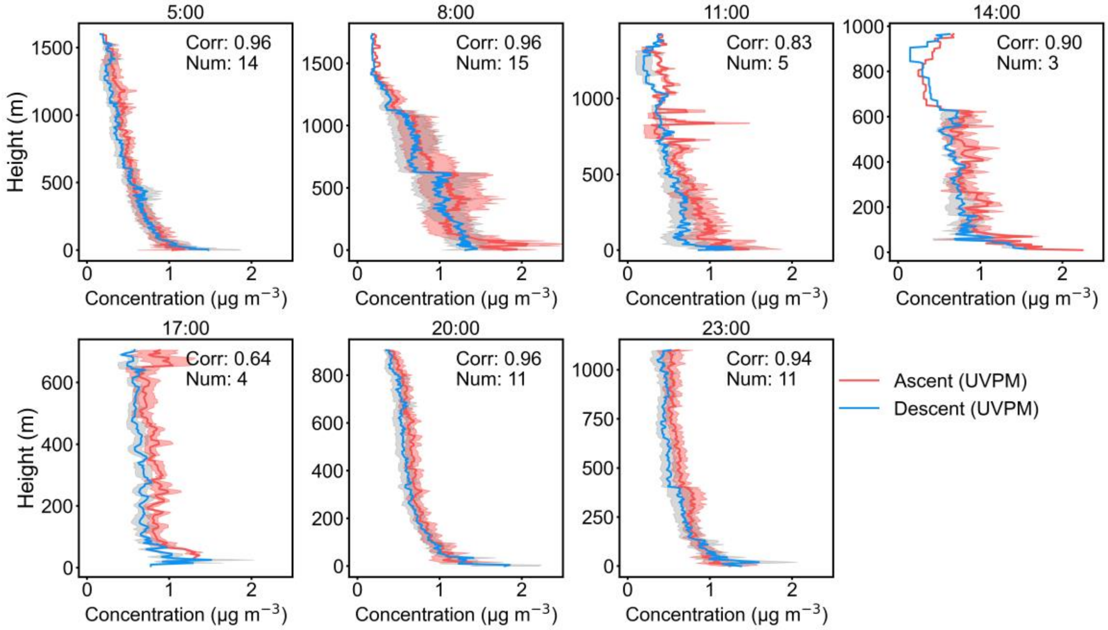

Figure S4. Comparison of ultraviolet-absorbing particulate matter (UVPM) vertical profiles during ascent with those during descent of the tethered balloon.

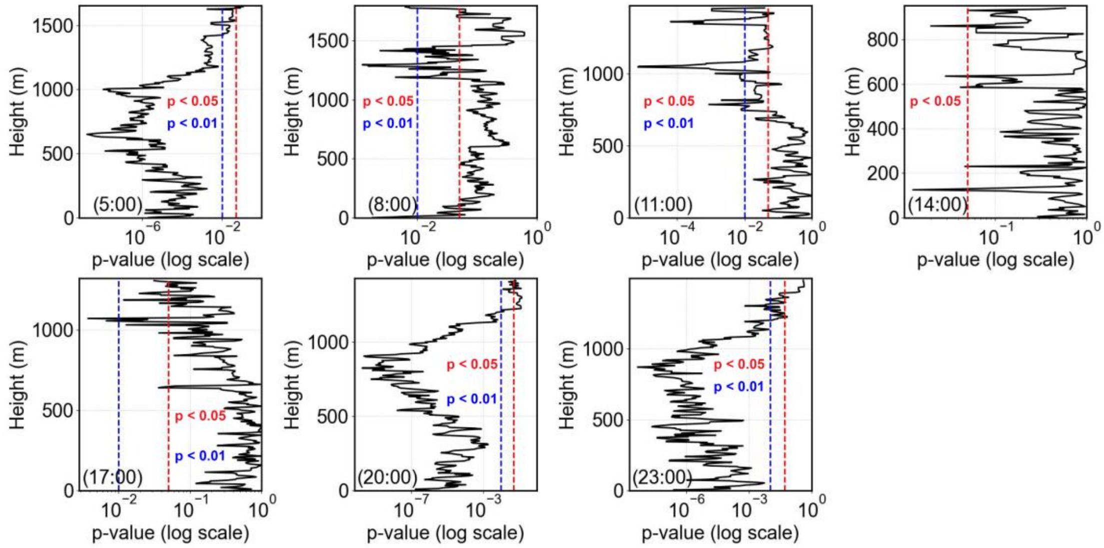

Figure S5. Significance test of the UVPM–eBC differences during different hours of the day. The red and blue dashed lines in the figure indicate p-values of 0.05 and 0.01, respectively.

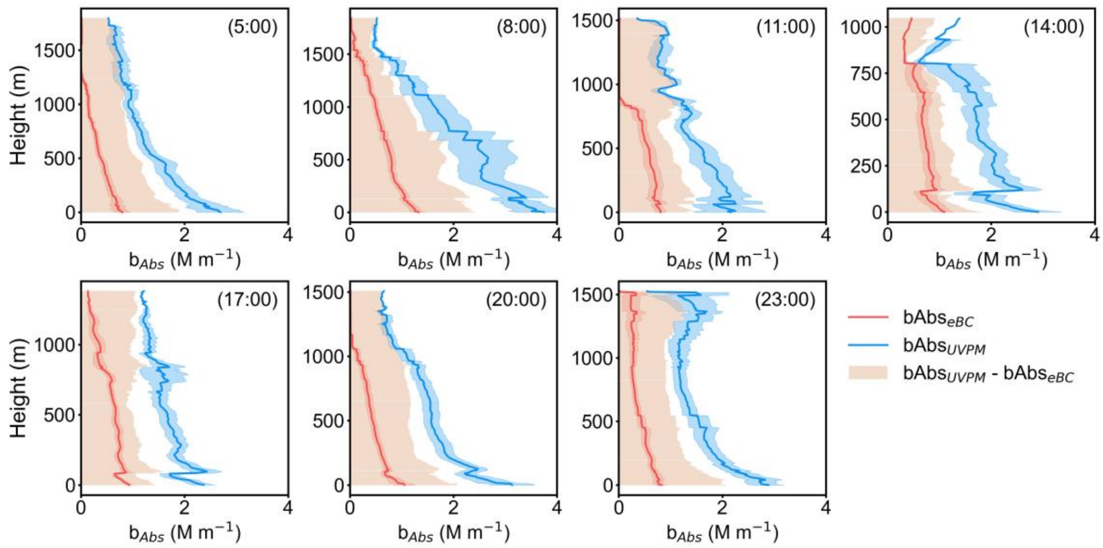

Figure S6. Diurnal variations in vertical profiles of the light absorption coefficients for UVPM and eBC at the Pingliang observation station during the summers of 2023 and 2024. The blue line and shaded area represent the mean profile and standard deviation of the UVPM light absorption coefficient, respectively. The red line and shaded area represent the mean profile and standard deviation of the eBC light absorption coefficient, respectively. The light orange shaded area indicates the difference between the light absorption coefficients of UVPM and eBC.

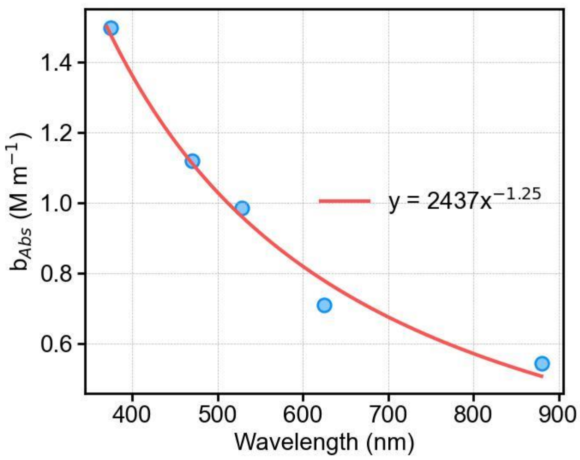

Figure S7. Example of Absorption Ångström Exponent (AAE) fitting calculation. The fitting equation is $b_{Abs}(\lambda) = k \times \lambda^{-AAE}$, where 2437 is the fitted value of k, and -1.25 is the fitted AAE value.

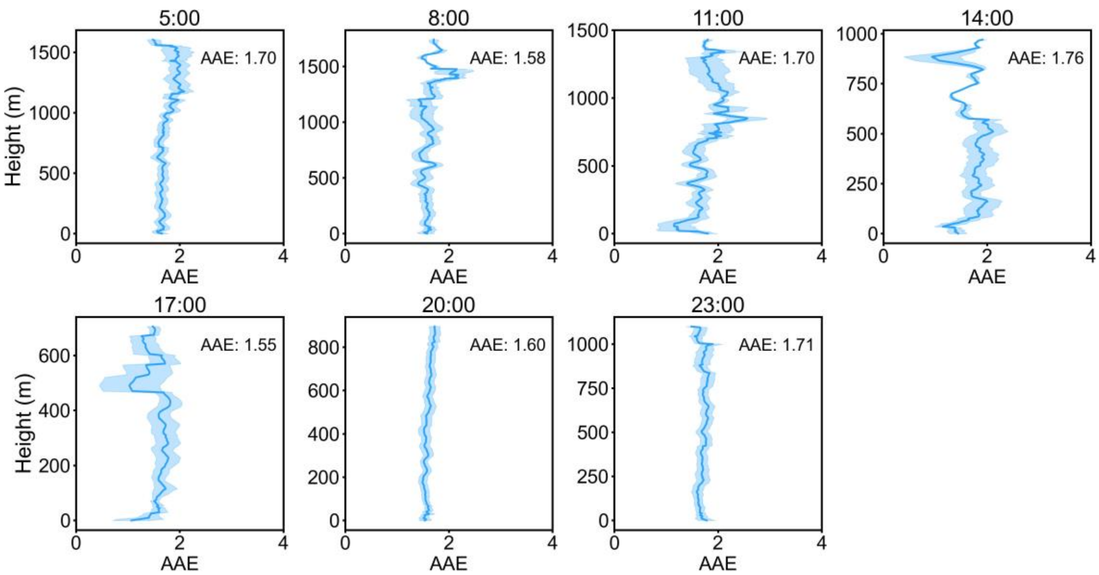

Figure S8. Mean diurnal variation of the vertical profiles of the Absorption Ångström Exponent for carbonaceous aerosols. The line and shaded area represent the mean profile and standard deviation of the AAE, respectively.

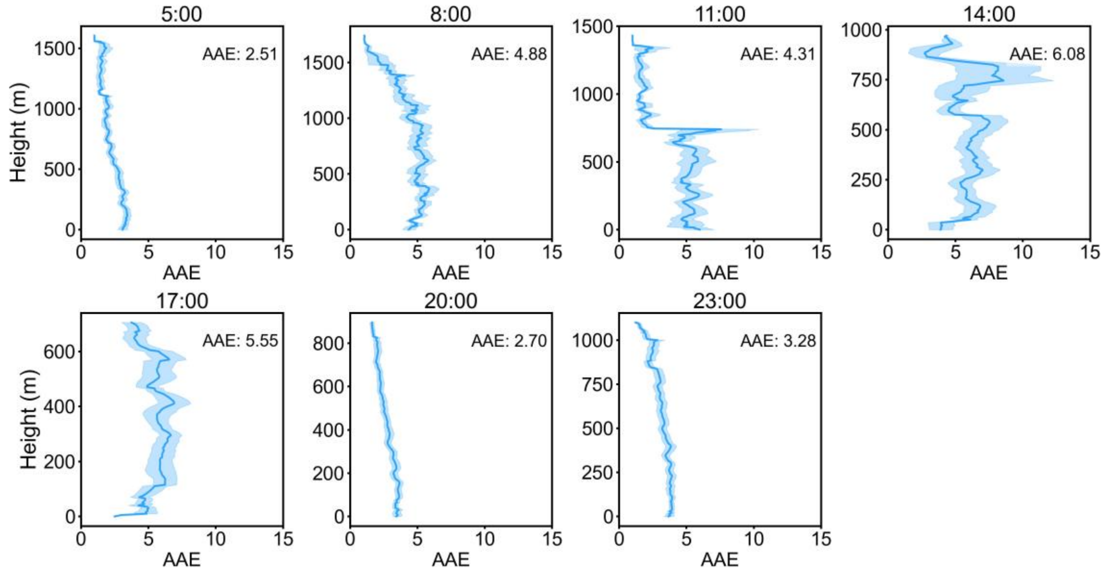

Figure S9. Mean diurnal variation of the vertical profile of Absorption Ångström Exponent for UVPM. The line and shaded area represent the mean profile and standard deviation of the AAE_{UVPM}, respectively.

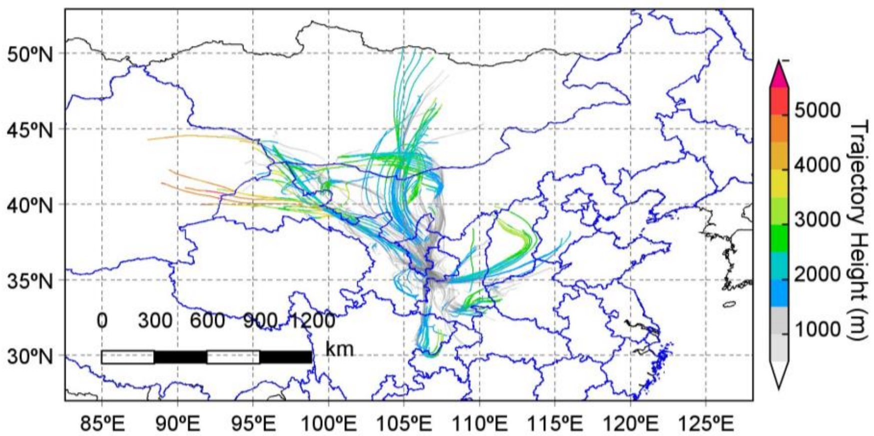

Figure S10. All 48-hour backward trajectories of air masses that reached the Pingliang Observatory at 500 m height (above ground level) during the measurement period (from July 15 to 24, 2023, and from July 17 to 31, 2024), where the different colors of each trajectory represent the altitude of the air mass at different geographic locations.

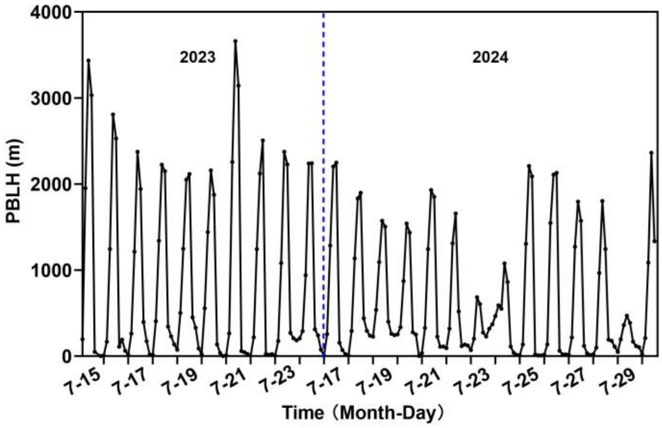

Figure S11. Temporal variation of the planetary boundary layer height over Pingliang urban area during the observation period (PBLH obtained from the Global Data Assimilation System). The observations in the year of 2023 and 2024 were separated by the vertical blue dashed line.

References

Chen, L.W.A., Chow, J.C., Wang, X.L., Robles, J.A., Sumlin, B.J., Lowenthal, D.H., Zimmermann, R., and Watson, J.G.: Multi-wavelength optical measurement to enhance thermal/optical analysis for carbonaceous aerosol. Atmos. Meas. Tech., 8(1), 451-461, https://doi.org/10.5194/amt-8-451-2015, 2015.

Chow, J.C., Watson, J.G., Green, M.C., Wang, X.L., Chen, L.-W.A., Trimble, D.L., Cropper, P.M., Kohl, S.D., and Gronstal, S.B.: Separation of brown carbon from black carbon for IMPROVE and CSN PM2.5 samples, Air Waste Manag. Assoc., 68(5), 494-510, https://doi.org/10.1080/10962247.2018.1426653, 2018.

Holzworth, G. C.: Estimates of mean maximum mixing depths in the contiguous united states. Mon. Weather Rev., 92(5), 235-242, http://doi.org/10.1175/1520-0493(1964)092<0235:EOMMMD>2.3.CO;2, 1964.

Wang, Y. Q.: MeteoInfo: GIS software for meteorological data visualization and analysis. Meteorol. Appl., 21(2), 360-368. http://doi.org/10.1002/met.1345, 2014.

Zhang, H. S., Zhang, X. Y., Li, Q. H., Cai, X. H., Fan, S. J., Song, Y., Hu, F., Che, H. Z., Quan, J. N., Kang, L., and Zhu, T.: Research progress on estimation of atmospheric boundary layer height. Acta Meteorol. Sin., 78(3), 522-536, http://doi.org/10.11676/qxxb2020.044,

2020.